Inorg. Chem. **2007**, *46*, 2530−2540

Synthesis and Voltammetry of $[bmim]_4[\alpha\text{-}S_2W_{18}O_{62}]$ and Related Compounds: Rapid Precipitation and Dissolution of Reduced Surface Films

Andrew W. A. Mariotti,[†,‡] Jingli Xie,[†,‡] Brendan F. Abrahams,[†] Alan M. Bond,*[,§] and Anthony G. Wedd*[,†,‡]

School of Chemistry, The University of Melbourne, 3010 Victoria, Australia, The Bio21 Molecular Science and Biotechnology Institute, Parkville, Victoria 3010, Australia, and The School of Chemistry, Monash University, Clayton, Victoria 3800, Australia

Received October 22, 2006

1-*n*-Butyl-3-methylimidazolium (bmim) salts of $[\alpha\text{-}SiM_{12}O_{40}]^{4-}$ and $[\alpha\text{-}S_2M_{18}O_{62}]^{4-}$ (M = Mo, W) were synthesized and characterized. In sharp contrast to the multiple one-electron diffusion-controlled reduction processes expected in solution at a glassy carbon electrode, reduction of these salts beyond the one-electron level in CH_3CN (0.1 M $[bmim][PF_6]$) led to rapid precipitation of arrays of microdroplets or microcrystals onto the surface. Upon oxidation these arrays dissolved on the electrochemical time scale, resulting in voltammograms displaying both diffusion-controlled and surface-confined behavior. These novel observations appear to be related to the ability of the $[bmim]^+$ cations and polyoxometalate anions to form ion clusters in solution and to the lower solubilities of the reduced salts.

Introduction

The chemistry of polyoxometalate anions has been studied widely as they have a rich variety of structural, redox, and catalytic properties.[1−5] Voltammetry has revealed that their reversible potentials are highly dependent on the nature of the solvent, supporting electrolyte, and proton concentration.[6,7] In particular, the cation in the supporting electrolyte, which is normally present in excess, influences behavior, presumably via ion clustering with the anions.[1,8−11] These effects appear to influence the catalytic and aggregation behavior of the anions, as well as their voltammetry.

The use of room-temperature ionic liquids in electrochemistry is becoming increasingly popular. These media act as both solvent and supporting electrolyte and can possess many useful properties such as large potential windows, negligible vapor pressure, high chemical and thermal stability, and an ability to dissolve a wide range of compounds.[12−18] The advantages have been seen in voltammetric studies of polyoxometalate anions in the ionic liquid $[bmim][PF_6]$ (bmim = 1-*n*-butyl-3-methylimidazolium) carried out in these laboratories.[19]

* To whom correspondence should be addressed. E-mail: agw@unimelb.edu.au (A.G.W.), alan.bond@sci.monash.edu.au (A.M.B.).
† The University of Melbourne.
‡ The Bio21 Institute.
§ Monash University.

(1) Hill, C. L. in *Comprehensive Coordination Chemistry II*; McCleverty, J. A., Meyer, T. J., Eds.; Elsevier: Amsterdam, 2004; Vol. 4, pp 679−759.
(2) Hill, C. L.; Prosser-McCartha, C. M. *Coord. Chem. Rev.* **1995**, *143*, 407−55.
(3) Hiskia, A.; Mylonas, A.; Papaconstantinou, E. *Chem. Soc. Rev.* **2001**, *30*, 62−69.
(4) Pope, M. T. *Heteropoly and Isopoly Oxometalates*; Springer-Verlag: Berlin, Heidelberg, Germany, 1983.
(5) Issue devoted to polyoxometalate chemistry: *Chem. Rev.* **1998**, *98*, 1−387.
(6) Chiang, M.-H.; Dzielawa, J. A.; Dietz, M. L.; Antonio, M. R. *J. Electroanal. Chem.* **2004**, *567*, 77−84.
(7) Sadakane, M.; Steckhan, E. *Chem. Rev.* **1998**, *98*, 219−237.
(8) Grigoriev, V. A.; Cheng, D.; Hill, C. L.; Weinstock, I. A. *J. Am. Chem. Soc.* **2001**, *123*, 5292−5307.
(9) Grigoriev, V. A.; Hill, C. L.; Weinstock, I. A. *J. Am. Chem. Soc.* **2000**, *122*, 3544−3545.
(10) Kirby, J. F.; Baker, L. C. W. *Inorg. Chem.* **1998**, *37*, 5537−5543.
(11) Carloni, P.; Eberson, L. *Acta Chem. Scand.* **1991**, *45*, 373−6.
(12) Buzzeo, M. C.; Evans, R. G.; Compton, R. G. *Chem. Phys. Chem.* **2004**, *5*, 1106−1120.
(13) Dupont, J.; de Souza, R. F.; Suarez, P. A. Z. *Chem. Rev.* **2002**, *102*, 3667−3691.
(14) Sheldon, R. *Chem. Commun.* **2001**, 2399−2407.
(15) Wasserscheid, P.; Keim, W. *Angew. Chem., Int. Ed.* **2000**, *39*, 3772−3789.
(16) Welton, T. *Chem. Rev.* **1999**, *99*, 2071−2083.
(17) Welton, T. *Coord. Chem. Rev.* **2004**, *248*, 2459−2477.
(18) Zhang, J.; Bond, A. M. *Analyst* **2005**, *130*, 1132−1147.

10.1021/ic062022d CCC: $37.00
Published on Web 03/09/2007

The voltammetry of certain Keggin anions (structure 1) in neat ionic liquids and in CH_3CN (with the ionic liquid present as the supporting electrolyte) was reported recently.[6] Reversible potentials were more positive in CH_3CN with [emim][BF_4] (emim = 1-*n*-ethyl-3-methylimidazolium**)** or [C_5mim][BF_4] (C_5mim = 1-*n*-pentyl-3-methylimidazolium) present as supporting electrolytes compared to [Bu_4N][PF_6]. The observations are consistent with stronger ion clustering in the presence of the former cations. Moreover, the use of neat [emim][BF_4] or [C_5mim][BF_4] caused the potentials to be more positive than those found in CH_3CN, regardless of electrolyte. This was attributed to the varying donor−acceptor properties of the solvents and to a greater degree of ion clustering induced by the higher effective concentration of cations. It is apparent that tuning of redox potentials may be possible via systematic variation of the solvent, from the pure ionic liquid to the pure organic solvent (with the ionic liquid present as the supporting electrolyte).

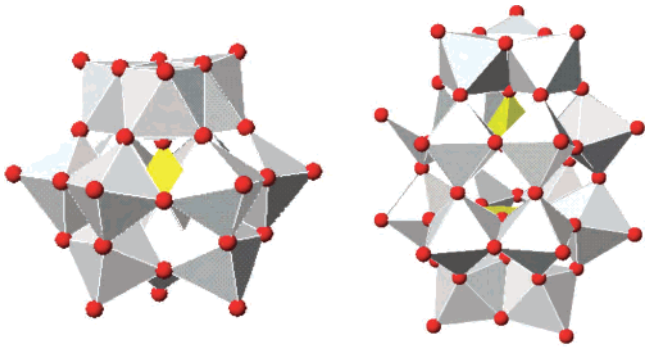

Structure I $[XM_{12}O_{40}]^{n-}$ Structure II $[XM_{18}O_{62}]^{n-}$

This work reports the voltammetry of the new salts [bmim]$_4$[α-$SiM_{12}O_{40}$] and [bmim]$_4$[α-$S_2M_{18}O_{62}$] (M = Mo, W) which feature the classic Keggin and Wells−Dawson anions (structures I and II, respectively),[4] as well as structural aspects of [bmim]$_4$[α-$S_2W_{18}O_{62}$]. Voltammetry in CH_3CN (containing either 0.1 M [bmim][PF_6] or [Bu_4N][PF_6] as the supporting electrolyte) is compared with those of the $[Bu_4N]^+$ salts under the same conditions.[19−22] Interesting effects caused by rapid precipitation and dissolution of reduced salts were observed which provide insight into the role of the $[bmim]^+$ cation in ion clustering and solubility. In particular, this behavior is consistent with the reduced salts themselves precipitating as arrays of microdroplets or microcrystals on the glassy carbon electrode.

Experimental Section

Reagents. Acetone ($(CH_3)_2CO$); Merck, AR), acetonitrile (CH_3CN; Ajax FineChem, UV anhydrous, 99.9%), 1,1′-diacetylferrocene ([$Fe(CpCOCH_3)_2$]; Aldrich, 97%), ethanol (EtOH; Merck, AR), ferrocene ([$FeCp_2$]; BDH), nitric acid (HNO_3; BDH), sodium metasilicate (Na_2SiO_3; Aldrich), sodium molybdate dihydrate (Na_2MoO_4·$2H_2O$; APS Ajax Finechem), sodium tungstate dihydrate (Na_2WO_4·$2H_2O$; APS Ajax Finechem), and sulfuric acid (H_2SO_4; BDH) were all used as supplied by the manufacturer. For voltammetric experiments, acetonitrile was dried and purified as in previous work.[19] [Bu_4N][PF_6] (Aldrich; 98%) was recrystallized twice from ethanol before use.[25] Syntheses of K_4[α-$SiW_{12}O_{40}$], [bmim]Cl, and [bmim][PF_6] followed literature procedures.[19,26] IR and NMR for [bmim][PF_6], were equivalent to those reported previously.[13,14,16,19,27,28]

Safety Consideration. The ionic liquid [bmim][PF_6] hydrolyzes to toxic compounds such as HF.[29] It is recommended that care be taken when handling this substance. Storage in a plastic vessel is recommended as it degrades glassware over time.

[bmim]$_4$[α-$SiMo_{12}O_{40}$]. HNO_3 (7.5 mL, 15.8 M) was added dropwise to a stirred solution of Na_2MoO_4·$2H_2O$ (5.50 g, 22.7 mmol) in water (30 mL). A solution of Na_2SiO_3 (0.25 g, 2.03 mmol) in water (10 mL) was added similarly and the mixture heated for 30 min on a steam bath with occasional swirling. A solution of [bmim]Cl (1.50 g, 8.53 mmol) in water (2 mL) was added similarly to the warm stirred solution providing an immediate yellow precipitate. After cooling in an ice/water bath, the solid was collected on a glass frit and washed with water (until the washings were neutral) and then ethanol. The crude product was recrystallized from acetone−water (4:1 v:v) followed by slow evaporation at room temperature. The yellow needles were collected on a glass frit, washed with water and ethanol, and dried under vacuum overnight (3.54 g, 79%), mp 326 °C (dec). Anal. Found: C, 16.34; H, 2.53; Mo, 47.9; N, 4.73. Calcd for $C_{32}H_{60}Mo_{12}N_8O_{40}Si$: C, 16.17; H, 2.55; Mo, 48.45; N, 4.72. Mass spectrum (ESI): +ve ion, *m*/*z* 139, $[bmim]^+$; −ve ion, *m*/*z* 486 = 1944/4, $[SiMo_{12}O_{40}]^{4-}$. IR (KBr disk): 3141, 3109, 2958, 2872, 1561, 1468, 1163, 989, 952, 901, 861, 790, 620, 533, 506 cm^{-1}. ^1H NMR (CH_3CN-d_3) [δ (ppm)]: 8.48 (s), 7.40 (d), 4.22 (t), 3.90 (s), 1.84 (m), 1.35 (m), 0.95 (t).

[bmim]$_4$[α-$SiW_{12}O_{40}$]. A solution of [bmim]Cl (1.50 g, 8.53 mmol) in water (2 mL) was added dropwise to a stirred solution of K_4[α-$SiW_{12}O_{40}$] (5.74 g, 1.90 mmol) in water (50 mL). The precipitated white solid was collected on a glass frit and washed with water and ethanol. The crude product was recrystallized from acetone−water (4:1 v:v) followed by slow evaporation at room temperature. The white needles were collected, washed with water and ethanol, and dried under vacuum overnight (5.98 g, 92%), mp 340 °C (dec). Anal. Found: C, 11.19; H, 1.68; N, 3.22. Calcd for $C_{32}H_{60}N_8O_{40}SiW_{12}$: C, 11.20; H, 1.76; N, 3.27. Mass spectrum (ESI): +ve ion, *m*/*z* 139, $[bmim]^+$; −ve ion, *m*/*z* 1438 = 2876/2, $[SiW_{12}O_{38}(OH)_2]^{2-}$. IR (KBr disk): 3141, 3109, 2958, 2872, 1561, 1468, 1164, 1014, 974, 920, 884, 792, 620, 534 cm^{-1}. ^1H NMR (CH_3CN-d_3) [δ (ppm)]: 8.49 (s), 7.38 (d), 4.21 (t), 3.87 (s), 1.83 (m), 1.34 (m), 0.94 (t).

(19) Zhang, J.; Bond, A. M.; MacFarlane, D. R.; Forsyth, S. A.; Pringle, J. M.; Mariotti, A. W. A.; Glowinski, A. F.; Wedd, A. G. *Inorg. Chem.* **2005**, *44*, 5123−5132.
(20) Himeno, S.; Tatewaki, H.; Hashimoto, M. *Bull. Chem. Soc. Jpn.* **2001**, *74*, 1623−1628.
(21) Richardt, P. J. S.; Gable, R. W.; Bond, A. M.; Wedd, A. G. *Inorg. Chem.* **2001**, *40*, 703−709.
(22) Zhang, J.; Bond, A. M.; Richardt, P. J. S.; Wedd, A. G. *Inorg. Chem.* **2004**, *43*, 8263−8271.
(23) Way, D. M.; Bond, A. M.; Wedd, A. G. *Inorg. Chem.* **1997**, *36*, 2826−2833.
(24) Guo, S.-X.; Mariotti, A. W. A.; Schlipf, C.; Bond, A. M.; Wedd, A. G. *J. Electroanal. Chem.* **2006**, *591*, 7−18.
(25) Sawyer, D. T.; Sobkowiak, A.; Roberts, J. L. J. *Electrochemistry for Chemists*, 2nd ed.; Wiley: New York, 1995.
(26) Teze, A.; Herve, G. *Inorg. Synth.* **1990**, *27*, 85−96.
(27) Chun, S.; Dzyuba, S. V.; Bartsch, R. A. *Anal. Chem.* **2001**, *73*, 3737−41.
(28) Paulechka, Y. U.; Kabo, G. J.; Blokhin, A. V.; Vydrov, O. A.; Magee, J. W.; Frenkel, M. *J. Chem. Eng. Data* **2003**, *48*, 457−462.
(29) Swatloski, R. P.; Holbrey, J. D.; Rogers, R. D. *Green Chem.* **2003**, *5*, 361−363.

[bmim]$_4$[α-$S_2Mo_{18}O_{62}$]. H_2SO_4 (4.96 mL, 18 M) was added dropwise to a stirred solution of $Na_2MoO_4{\cdot}2H_2O$ (6.23 g, 25.7 mmol) in water (20 mL). CH_3CN (100 mL) was added, and the solution was refluxed for 1 h before cooling to room temperature. The lower layer was discarded, and the dark orange upper layer was collected and filtered through a fluted filter paper. A solution of [bmim]Cl (1.00 g, 5.73 mmol) in CH_3CN (5 mL) was added dropwise to the stirred orange solution. Most of the solvent was removed by rotary evaporation, and the orange solid was collected on a glass frit and washed with water (until the washings were neutral) and then with ethanol. The crude product was recrystallized from acetonitrile−water (1:1 v:v) followed by slow evaporation at room temperature. The orange crystals were collected, washed with water and ethanol, and dried under vacuum overnight (0.83 g, 17%), mp 315 °C (dec). Anal. Found: C, 12.00; H, 1.87; Mo, 51.90; N, 3.25; S, 1.89. Calcd for $C_{32}H_{60}Mo_{18}N_8O_{62}S_2$: C, 11.51; H, 1.81; Mo, 51.71; N, 3.36; S, 1.92. Mass spectrum (ESI): +ve ion, *m*/*z* 139, $[bmim]^+$; −ve ion, *m*/*z* 696 = 2784/4, $[S_2Mo_{18}O_{62}]^{4-}$. IR (KBr disk): 3141, 3109, 2958, 2872, 1561, 1468, 1168, 1069, 965, 786, 618, 420 cm^{-1}. ^1H NMR (CH_3CN-d_3) [δ (ppm)]: 8.42 (s), 7.39 (d), 4.18 (t), 3.86 (s), 1.83 (m), 1.35 (m), 0.96 (t). ^{13}C NMR (CH_3CN-d_3) [δ (ppm)]: 136.8, 124.8, 123.5, 50.5, 37.0, 32.7, 20.1, 13.8.

[bmim]$_4$[α-$S_2W_{18}O_{62}$]. CH_3CN (275 mL) was added to a stirred solution of $Na_2WO_4{\cdot}2H_2O$ (11.25 g, 31.4 mmol) in water (335 mL). H_2SO_4 (75 mL, 18 M) was added dropwise, after which the solution was stirred at 70 °C for 14 days. After the solution was cooled to room temperature, CH_3CN (200 mL) was added to provide two layers. The lower layer was discarded and the clear lime-green upper layer collected. A solution of [bmim]Cl (1.5 g, 8.5 mmol) in CH_3CN (3 mL) was added dropwise to the collected solution. Most of the solvent was removed by rotary evaporation and the green solid collected on a glass frit. The solids were washed with water until the washings were neutral and then with ethanol. The crude product was recrystallized from acetonitrile−water (1:1 v:v) followed by slow evaporation at room temperature. Green crystals were collected, washed with water and ethanol, and dried under vacuum overnight (4.33 g, 46%), mp 355 °C (dec). Anal. Found: C, 8.30; H, 1.25; N, 2.15; S, 1.28. Calcd for $C_{32}H_{60}N_8O_{62}S_2W_{18}$: C, 7.81; H, 1.23; N, 2.28; S, 1.30. Mass spectrum (ESI): +ve ion, *m*/*z* 139, $[bmim]^+$; −ve ion, *m*/*z* 1091 = 4364/4, $[S_2W_{18}O_{62}]^{4-}$. IR (KBr disk): 3141, 3109, 2958, 2872, 1561, 1468, 1179, 1075, 987, 968, 906, 795, 620, 511, 487 cm^{-1}. ^1H NMR (CH_3CN-d_3) [δ (ppm)]: 8.42 (s), 7.40 (d), 4.19 (t), 3.87 (s), 1.84 (m), 1.36 (m), 0.96 (t). ^{13}C NMR (CH_3CN-d_3) [δ (ppm)]: 136.8, 124.8, 123.4, 50.5, 37.0, 32.7, 20.1, 13.8.

Instrumentation and Procedures. Voltammetric experiments were performed with an Autolab (PGSTAT100) (Eco Chemie, Utrecht, Netherlands) computer-controlled electrochemical workstation. A standard three-electrode arrangement was employed with a 3 mm glassy carbon Metrohm 628-10 electrode used as the working electrode for both stationary and rotating disk experiments and a platinum wire used as the counter electrode. An Ag^+/Ag (CH_3CN, 10 mM $AgNO_3$) double junction electrode was used as the reference electrode, and potentials are quoted relative to the ferrocenium/ferrocene (Fc^+/Fc) scale, using either ferrocene (Fc) or 1,1′-diacetylferrocene ($E^{0\prime}$ = 458 mV vs Fc^+/Fc in CH_3CN (0.1 M $[Bu_4N][PF_6]$ or $[bmim]PF_6$])) as an internal reference.[30]

The effective area (6.31×10^{-2} cm^2) of the glassy carbon working electrode was determined by measurement of the peak current obtained for the reversible one-electron oxidation of ferrocene (1 mM) in CH_3CN (0.1 M $[Bu_4N][PF_6]$) under conditions of linear sweep voltammetry and use of the Randles−Sevcik equation:[31]

$$I_p = 0.4463nF\left(\frac{nF}{RT}\right)^{1/2}AD^{1/2}v^{1/2}C \quad (1)$$

Here, I_p is the peak current (A), n (=1) is the number of electron equivalents, A is the electrode area (cm^2), D is the diffusion coefficient (taken to be 2.3×10^{-5} cm^2 s^{-1}),[52] C is the concentration of ferrocene (mol cm^{-3}), v is the scan rate (V s^{-1}), and the other symbols have their usual meaning.

The procedure for mechanical attachment of microcrystalline solids onto electrode surfaces has been described in detail previously.[32] In brief, the relevant polyoxometalate salt was ground in a mortar and pestle and attached mechanically to the electrode surface via a cotton bud. The working electrode used in these solid-state voltammetric experiments was polished before attachment of the solid.

For electrochemical experiments conducted in CH_3CN, the electrolyte ($[Bu_4N][PF_6]$ or $[bmim][PF_6]$) was dried overnight at 100 or 50 °C, respectively, in a Schlenk tube under vacuum. The relevant solid polyoxometalate salt was dried similarly but at room temperature. In solution-phase experiments, all samples were subjected to four pump/N_2 fill cycles, before the required amount of dry CH_3CN was transferred from a solvent tower via a gastight syringe to the Schlenk tube containing the polyoxometalate salt. After dissolution, this solution was transferred via a gastight syringe to the tube containing the relevant electrolyte. This sample solution was transferred similarly to a flame-dried electrochemical cell (which had been cooled in a stream of N_2) and bubbled with dry N_2 for 15 min before undertaking voltammetric experiments. For solid-state voltammetric experiments, the procedure was similar, except that the relevant solid of interest was attached to the working electrode (as described above) after being dried at room temperature overnight under vacuum.

Before being inserted into the electrochemical cell, the counter electrode was flame-dried and the working electrode was polished with an Al_2O_3 (Buehler, 0.3 μm) slurry, rinsed with distilled water, sonicated, repolished, rinsed with water, ethanol, dried with a tissue, and then dried with a hot air blower. The reference electrode was rinsed with acetone and then ethanol, dried with a tissue, and dried with a hot air blower. At all times the electrochemical cell was kept under a positive pressure of N_2. When required, electrode removal was carried out under a flow of dinitrogen. The voltammetric experiments were conducted at ambient temperature (20 ± 2 °C).

NMR spectra were obtained with a Varian Unity 400 MHz instrument in acetonitrile-d_3, with 20% $CFCl_3$ (in acetone-d_6) and 85% H_3PO_4 (in D_2O) being used as external references for ^{19}F and ^{31}P NMR, respectively (set to 0 ppm). IR spectra were obtained with a Bio-Rad FTS 165 FT-IR spectrometer. Mass spectra (in CH_3CN) were collected using a Finnigan DecaXP max electrospray ionization mass spectrometer (ESI-MS). Elemental analyses were performed by The Campbell Microanalytical Laboratory, University of Otago, Otago, New Zealand.

X-ray Crystallography. Crystals of [bmim]$_4$[α-$S_2W_{18}O_{62}$] were grown by slow evaporation of an acetonitrile−acetone−water solution (1:1:1) at room temperature. Details of the structure solution are supplied in the Supporting Information. The crystal examined was strongly absorbing due to the relatively large number of

(30) Gritzner, G.; Kuta, J. *Pure Appl. Chem.* **1984**, *56*, 461−6.

(31) Bard, A. J.; Faulkner, L. R. *Electrochemical methods: fundamentals and applications*, 2nd ed.; Wiley: New York, 2001.

(32) Bond, A. M.; McLennan, E. A.; Stojanovic, R. S.; Thomas, F. G. *Anal. Chem.* **1987**, *59*, 2853−60.

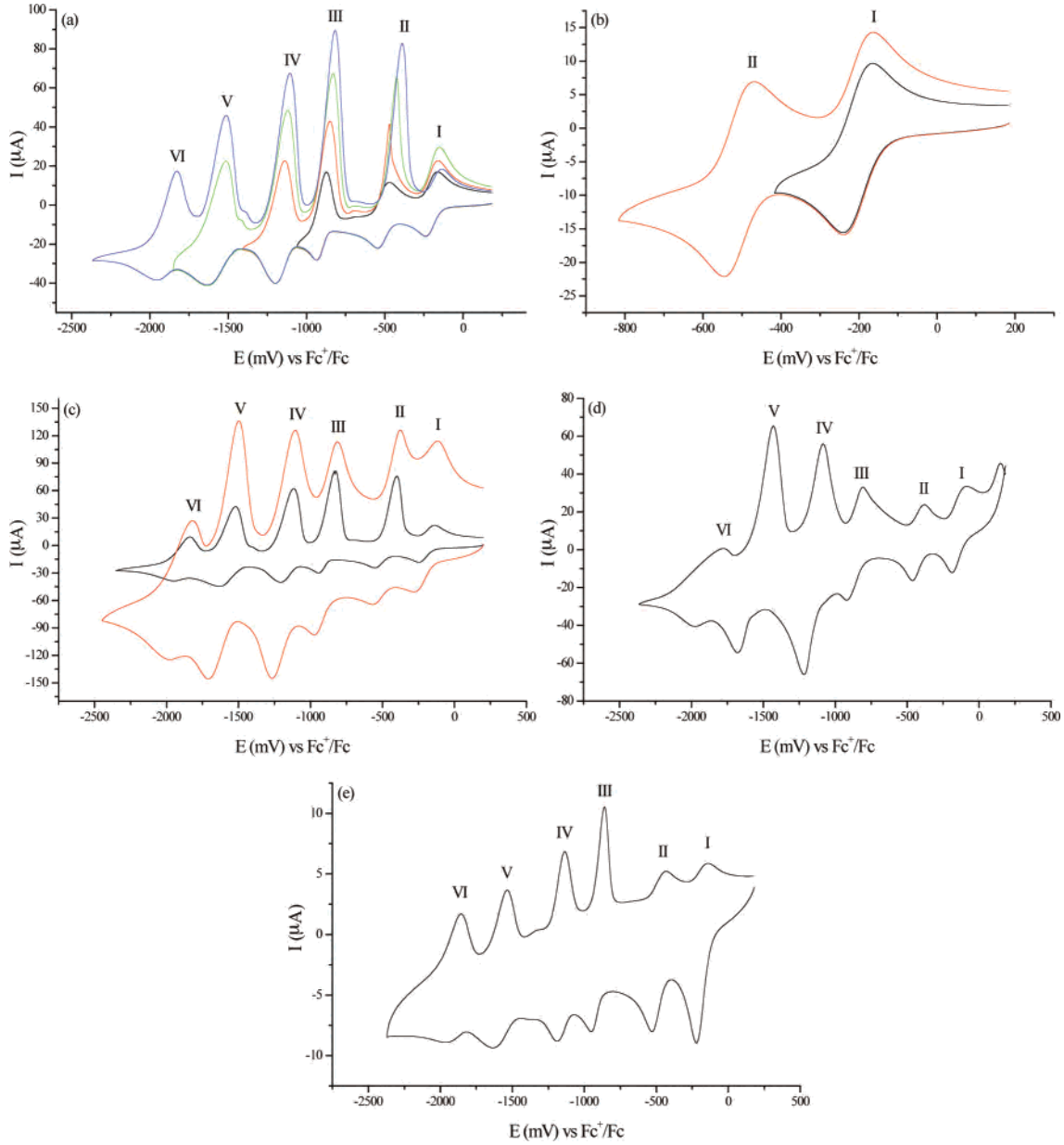

Figure 1. Cyclic voltammograms for [bmim]$_4$[α-$S_2W_{18}O_{62}$] (1 mM) at a glassy carbon electrode in CH_3CN ([bmim][PF_6], 0.1 M) with $\nu = 100$ mV s^{-1} unless stated otherwise: (a) potential switched after the third (black), fourth (red), fifth (green), and sixth (blue) processes; (b) potential switched after the first (black) and second (red) processes; (c) scan rates of 100 (black) and 1000 (red) mV s^{-1}; (d) 10th cycle in the potential range +200 to −2400 mV; (e) scan of the blue film deposited on the electrode (see text for further details).

Scheme 1

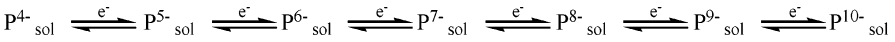

Scheme 2

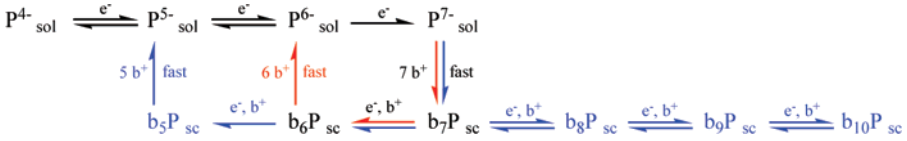

tungsten centers in the unit cell. As a consequence, the refinement of the structure was severely hampered. In particular, there were peaks of residual electron density in the Fourier difference maps near W centers, in some cases as intense as 8 e $Å^{-3}$ plus disorder in one of the cations. This led to a R1 factor of 0.1037 only (Table S1). Despite the difficulties, valuable structural information was discernible and is discussed below.

Results and Discussion

Synthesis and Structural Characterization. Syntheses of the $[bmim]^+$ salts of $[SiM_{12}O_{40}]^{4-}$ and $[S_2M_{18}O_{62}]^{4-}$ (M = Mo, W) were adapted from the methods which provided their tetraalkylammonium salts.[20,22,33,34] The presence of the α-isomer of the anion in [bmim]$_4$[$S_2W_{18}O_{62}$] (structure II;

Table 1. Cyclic Voltammetric Data[a] for the Reduction of $[bmim]_4[\alpha\text{-}S_2W_{18}O_{62}]$ (1 mM) in CH_3CN ($[bmim][PF_6]$, 0.1 M) at a Glassy Carbon Electrode

		process scanned to					
process	type	I	II	III	IV	V	VI
I	E_p^{ox}	−164	−165	−162	−160	−152	−136
	E_p^{red}	−240	−239	−238	−240	−238	−238
II	E_p^{ox}		−467	−472	−470	−423	−387
	E_p^{red}		−546	−545	−545	−545	−543
III	E_p^{ox}			−873	−851	−831	−816
	E_p^{red}			−936	−936	−936	−936
IV	E_p^{ox}				−1139	−1119	−1106
	E_p^{red}				−1197	−1197	−1197
V	E_p^{ox}					−1515	−1515
	E_p^{red}					−1637	−1634
VI	E_p^{ox}						−1827
	E_p^{red}						−1957

[a] E_p^{ox} and E_p^{red} (mV) vs Fc^+/Fc; $\upsilon = 100$ mV s^{-1}.

Figure S1) was confirmed by X-ray crystallography (see Supporting Information).

Voltammetry of $[Bu_4N]_4[S_2W_{18}O_{62}]$ in CH_3CN ($[Bu_4N][PF_6]$, 0.1 M). Six reversible, diffusion-controlled, one-electron solution-phase processes have been observed in the range +260 to −2670 mV (vs Fc^+/Fc) by cyclic voltammetry (see also Table 4).[19] This behavior is described by Scheme 1, where P represents $[S_2W_{18}O_{62}]$ and sol represents solution behavior. It is presumed that ion clustering reduces the effective anionic charge for each redox state.

Voltammetry of $[bmim]_4[S_2W_{18}O_{62}]$ in CH_3CN ($[bmim][PF_6]$, 0.1 M). Cyclic Voltammetry. The behavior at negative potentials was intriguingly different when $[bmim]^+$ replaced $[Bu_4N]^+$ as the only cation present. Sharp oxidation peaks were observed rather than the broader peak shapes characteristic of diffusion controlled processes (Figure 1a). However, the first reduction process I remained a reversible, diffusion-controlled, one-electron event (Figure 1b). For scan rates in the range 20−1000 mV s^{-1}, I_p^{ox}/I_p^{red} was close to unity and ΔE_p was 76 mV for a scan rate of 100 mV s^{-1}, indistinguishable from that obtained for the ferrocene reference standard under the same conditions. The difference from the theoretically predicted value of 56 mV at 20 °C can be attributed to a low level of uncompensated resistance.[31] Application of the Randles−Sevcik equation to process I allowed an estimation of the diffusion coefficient of 8.4×10^{-6} cm^2 s^{-1} to be made for the $[S_2M_{18}O_{62}]^{4-}$ anion under the experimental conditions.[51] Process II was also found to be a well-behaved, reversible, one-electron solution-phase process (Figure 1b; Table 1).

Behavior different from that observed with the $[Bu_4N]^+$ cation was first encountered when the third reduction step was included in the cyclic voltammetry (Figure 1a). The oxidation component of process III exhibited both a different shape and a significantly larger current than did the reduction step. Such features are often associated with surface confined voltammetry (e.g., at a thin film).[31] In contrast, when the potential was swept in the positive direction, the oxidation peaks associated with processes I and II retained their diffusion-controlled shapes (Figure 1a).

Table 2. Cyclic Voltammetric Data[a] for the Reduction of $[bmim]_4[\alpha\text{-}S_2W_{18}O_{62}]$ (1 mM) in CH_3CN ($[bmim][PF_6]$, 0.1 M) When Scanned to Process VI at a Glassy Carbon Electrode

		process					
υ[b]	type	I	II	III	IV	V	VI
100	E_p^{ox}	−137	−399	−825	−1116	−1520	−1839
	E_p^{red}	−247	−544	−945	−1206	−1633	−1950
1000	E_p^{ox}	−114	−375	−813	−1106	−1497	−1819
	E_p^{red}	−281	−569	−973	−1265	−1710	−1978

[a] E_p^{ox} and E_p^{red} (mV) vs Fc^+/Fc. [b] Scan rate (mV s^{-1}).

If the potential scan was halted at the switching point after process III, a blue film could be seen on the electrode surface. The film was absent if the potential was switched prior to the onset of process III. The behavior is attributed to precipitation of the $[bmim]^+$ salt of the three-electron reduced anion $[S_2W_{18}O_{62}]^{7-}$ onto the electrode surface, followed by its dissolution once the two-electron form is generated on the oxidative scan.

Analogous behavior was seen for processes IV to VI inclusive (Figure 1a), with a gradual buildup of surface-confined material detected as the switching potential became progressively more negative. When the potential was switched at potentials more negative than process III, the oxidation for process II also displayed surface confined characteristics. It should be noted that I_p^{red} for processes V and VI were smaller than might be expected. This may be attributed to increasing amounts of solid precipitating onto the electrode surface at higher levels of reduction, thereby decreasing the effective electrode surface area.

The E_p^{red} values (Table 1) for processes I to VI remained essentially constant regardless of the switching potential. In contrast, E_p^{ox} values (Figure 1a, Table 1) became increasingly less negative as the degree of reduction increased.

A representation of this complex voltammetric behavior under the conditions of Figure 1a and Table 1 is given in Scheme 2 (b represents [bmim], sc represents surface-confined, and the other symbols are those given in Scheme 1). One- or two-electron reduction of $[S_2W_{18}O_{62}]^{4-}$ occurs via solution-phase voltammetry. Further reduction led to surface-confined behavior, but dependent upon the extent of reduction, different pathways were detected. Three-electron reduction led to the red pathway (Scheme 2). Further reduction led to the blue pathway. The reasons for this difference but may be attributed to buildup of material on the electrode surface for longer time scales (see discussion below). It should be noted that the above scheme is simplified and that multiple $[bmim]^+$ cations may be associated with the anions via ion clustering in solution.

An increase in the scan rate from 100 to 1000 mV s^{-1} increased the peak currents (Figure 1c). E_p^{red} values became more negative, and E_p^{ox} values, more positive (Table 2). I_p^{red} is proportional to $\upsilon^{1/2}$ for a diffusion-controlled process but proportional to υ for a surface confined process.[51] The relatively larger increase in I_p^{red} for the more negative processes was consistent with these containing surface-

(33) Rocchiccioli-Deltcheff, C.; Fournier, M.; Franck, R.; Thouvenot, R. *Inorg. Chem.* **1983**, *22*, 207−16.
(34) Sanchez, C.; Livage, J.; Launay, J. P.; Fournier, M.; Jeannin, Y. *J. Amer. Chem. Soc.* **1982**, *104*, 3194−202.

Table 3. Comparison of Cyclic Voltammetric Data[a] for the Blue Solid Film Formed on the Glassy Carbon Electrode upon Reduction of [bmim]$_4$[α-$S_2W_{18}O_{62}$] (1 mM) in CH_3CN ([bmim][PF_6], 0.1 M) upon Scanning to Process VI

		process					
species	type	I	II	III	IV	V	VI
blue solid	E_p^{ox}	−140	−431	−861	−1134	−1537	−1857
	E_p^{red}	−221	−529	−953	−1186	−1638	−1967
[bmim]$_4$[a-$S_2W_{18}O_{62}$]	E_p^{ox}	−137	−399	−825	−1116	−1520	−1839
	E_p^{red}	−247	−544	−945	−1206	−1633	−1950

[a] E_p^{ox} and E_p^{red} (mV) vs Fc^+/Fc; $\upsilon = 100$ mV s^{-1}.

confined components. Evidence of the effects of increased IR drop also was present at higher scan rates.

Multiple potential cycling through the range +200 to −2400 mV caused significant changes to the observed voltammograms (Figure 1d shows the situation after 10 cycles). This is attributed again to buildup of material on the electrode surface. Interestingly, brief stirring of the solution after repetitive cycling restored the original voltammogram.

To confirm that a condensed phase (blue film) was deposited on the electrode surface, the glassy carbon electrode was held at a potential of −2340 mV for 10 s in a solution containing [bmim]$_4$[α-$S_2W_{18}O_{62}$] (1 mM) in CH_3CN ([bmim][PF_6], 0.1 M). The electrode was then removed from solution, dried with a tissue, and placed in contact with a fresh electrolyte solution. The voltammetry (Figure 1e) still retained the six processes seen in Figure 1a, but the relative peak heights were different and peak currents were much smaller. Nevertheless, the E_p^{ox} and E_p^{red} values were the same within experimental error as those seen for the initial response for a starting solution (Table 3). These results are consistent with the formation of surface-confined material of approximate stoichiometry [bmim]$_{10}$[$S_2W_{18}O_{62}$] at very negative potentials.

If the potential was held for 20 s or more, a distorted response or no response was detected. Apparently the electrode coating became too thick and large IR distortion was encountered. This outcome is consistent with previous solid-state experiments with ferrocene where the voltammetry was strongly dependent on amount of compound adhered to the electrode surface.[35]

Rotated Disk Electrode Voltammetry. Under these conditions at low scan rates, a sigmoidal-shaped response should be detected for solution-phase processes.[31] RDE voltammograms for the reduction of [bmim]$_4$[α-$S_2W_{18}O_{62}$] in CH_3CN ([bmim][PF_6], 0.1 M) are displayed in Figure 2. The response for process I was sigmoidal in shape (Figure 2a). A plot of I_L vs $\omega^{1/2}$ was linear, indicative of a mass transport controlled reversible process.

A diffusion coefficient of 6.6×10^{-6} cm^2 s^{-1} was determined by application of the Levich Equation,[21] which is slightly smaller than that obtained from the cyclic voltammetry but slightly larger than that reported for [Bu_4N]$_4$[$S_2W_{18}O_{62}$] in CH_3CN ([Bu_4N][ClO_4], 0.1 M) from RDE voltammetry.[21] A plot of E vs $\ln[(I_L - I)/I]$ was linear, and the gradient provided a value of $n = 0.9$ electron equiv, consistent with previous studies.[21]

Process II, similar in shape and I_L value to process I, was observed at more negative potentials (Figure 2a). The limiting currents for processes I and II at a rotation rate of 3000 rpm were 61 and 58 μA, respectively, indicating that process II is also a one-electron step. However, some hysteresis was detected in the limiting current potential region when the potential was switched (Figure 2a). This may be attributed to a small amount of film formation due to the higher rate of mass transport and the slower scan rates used under RDE conditions relative to those for cyclic voltammetry.

Under RDE conditions, process III exhibited major distortion and hysteresis (Figure 2b). However, the sigmoidal shape was recovered once the potentials for process II were reached on the reverse scan. A small positive current was detected at potentials more positive than process I (Figure 2b), consistent with the presence of reduced forms of the anion generated either electrochemically or chemically via the reduction of $[S_2W_{18}O_{62}]^{4-}$(soln) by reduced solid. The extensive film formation now encountered produced large IR drop effects (Figure 2b). Process III led to electrode coating analogous to that encountered in the cyclic voltammetry. However, the extent of film formation was enhanced by the higher rate of mass transport and longer deposition time (i.e., slower scan rate) characteristic of RDE voltammetry.

If the potential was switched at a value appropriate for process VI, hysteresis was dominant (Figure 2b). Extensive bulk electrolysis was observed in these experiments as the position of the baseline current shifted from 0 to 10 μA after a complete scan. However, even though extensive film formation occurred, resumption of the sigmoidal shape commenced before the onset of process I on the reverse scan direction, indicating that dissolution of the precipitated film was rapid under these RDE voltammetric conditions.

Cyclic Voltammetry of [bmim]$_4$[$S_2W_{18}O_{62}$] in CH_3CN with Supporting Electrolyte [Bu_4N][PF_6] (0.1 M). Although the salt is sparingly soluble in CH_3CN (0.1 M [Bu_4N][PF_6]), six reduction processes were still observed in the cyclic voltammograms (Figure 3) and the data obtained are listed in Table 4. When the scan range was limited to processes I to IV inclusive, the data were consistent with solution-phase voltammetry. However, if the scan range included processes V and VI, the oxidation component of process IV exhibited a significantly higher current than its reductive counterpart (Figure 3).

The results implied that $[Bu_4N]^+$ salts were more soluble in CH_3CN than their $[bmim]^+$ analogues, but low solubility still affected the behavior of $[S_2W_{18}O_{62}]^{7-}$ and more highly reduced anions. The behavior of [bmim]$_4$[$S_2W_{18}O_{62}$] in CH_3CN ([Bu_4N][PF_6], 0.1 M) may be described by Scheme 3, where t represents [Bu_4N] and the other symbols are defined in Schemes 1 and 2.

(35) Zhang, J.; Bond, A. M. *Anal. Chem.* **2003**, *75*, 2694−2702.

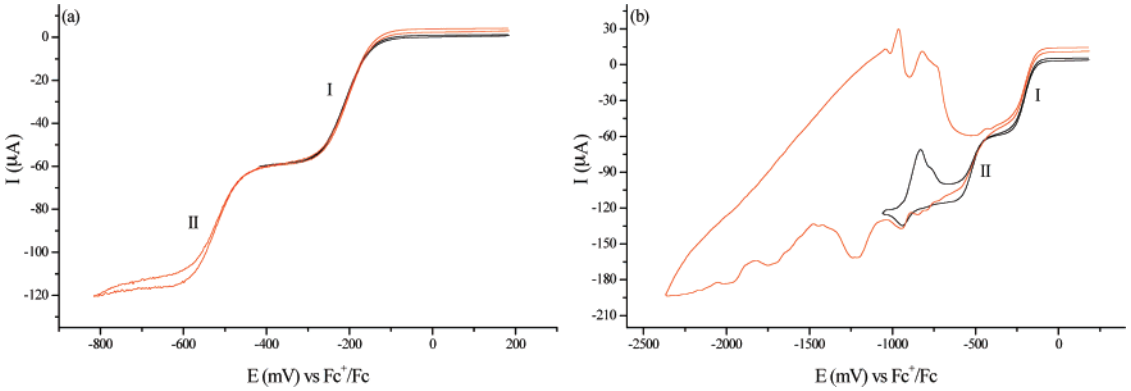

Figure 2. RDE voltammograms ($N = 3000$ rpm, $\upsilon = 10$ mV s^{-1}) obtained for $[bmim]_4[\alpha\text{-}S_2W_{18}O_{62}]$ (1 mM) in CH_3CN ($[bmim][PF_6]$, 0.1 M) at a glassy carbon electrode when the potential was switched after the (a) first (black) and second (red) and (b) third (black) and sixth (red) processes.

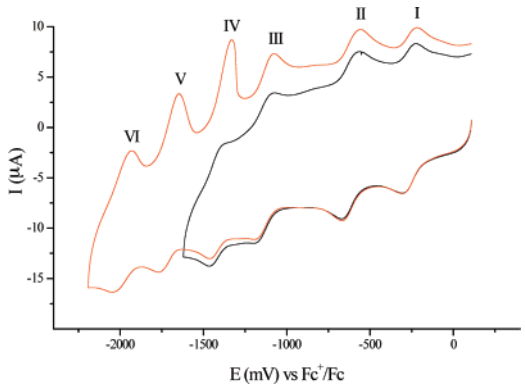

Figure 3. Cyclic voltammograms ($\upsilon = 100$ mV s^{-1}) for $[bmim]_4[\alpha\text{-}S_2W_{18}O_{62}]$ (saturated solution) in CH_3CN ($[Bu_4N][PF_6]$, 0.1 M) at a glassy carbon electrode when the potential was switched after processes IV (black) and VI (red).

Table 4. Cyclic Voltammetric Data[a] for the Reduction of $[X]_4[\alpha\text{-}S_2W_{18}O_{62}]$ (1 mM) in CH_3CN ($[Y][PF_6]$, 0.1 M) upon Scanning to Process VI at a Glassy Carbon Electrode

			process					
X	Y	type	I	II	III	IV	V	VI
$[bmim]^+$	$[bmim]^+$	E_p^{ox}	−137	−399	−825	−1116	−1520	−1839
		E_p^{red}	−247	−544	−945	−1206	−1633	−1950
	$[Bu_4N]^+$[b]	E_p^{ox}	−220	−557	−1076	−1330	−1648	−1931
		E_p^{red}	−306	−670	−1194	−1462	−1770	−2043
$[Bu_4N]^+$	$[bmim]^+$	E_p^{ox}	−154	−410	−820	−1104	−1506	−1833
		E_p^{red}	−237	−545	−933	−1192	−1643	−1936
	$[Bu_4N]^+$	E_p^{ox}	−199	−574	−1146	−1549	−2039	−2416
		E_p^{red}	−292	−682	−1251	−1642	−2149	−2511

[a] E_p^{ox} and E_p^{red} (mV) vs Fc^+/Fc; $\upsilon = 100$ mV s^{-1}. [b] Saturated solution.

Both E_p^{ox} and E_p^{red} values with $[Bu_4N][PF_6]$ (0.1 M) as electrolyte were significantly more negative compared to those found in the case when $[bmim][PF_6]$ (0.1 M) acted as electrolyte (Table 4). These data imply that ion clustering was significantly more important for $[bmim]^+$ than for $[Bu_4N]^+$. The significantly greater solubility of $[Bu_4N]^+$ salts relative to their $[bmim]^+$ counterparts probably also reflects this fact.

Cyclic Voltammetry of $[Bu_4N]_4[S_2W_{18}O_{62}]$ (1.0 mM) in CH_3CN with Supporting Electrolyte $[bmim][PF_6]$ (0.1 M). This combination provided a concentration of 0.1 M $[bmim]^+$ but only 0.004 M $[Bu_4N]^+$ in the CH_3CN phase. The behavior was expected to be similar to that observed when $[bmim]^+$ was the sole cation present, and the results displayed in Figure 4a and data summarized in Table 5 essentially confirm the prediction.

Table 5. Cyclic Voltammetric Data[a] for the Reduction of $[Bu_4N]_4[\alpha\text{-}S_2W_{18}O_{62}]$ (1 mM) in CH_3CN ($[bmim][PF_6]$, 0.1 M) at a Glassy Carbon Electrode

		process scanned to					
process	type	I	II	III	IV	V	VI
I	E_p^{ox}	−169	−161	−161	−159	−154	−154
	E_p^{red}	−251	−237	−237	−237	−237	−237
II	E_p^{ox}		−469	−469	−463[b]	−434[b]	−410
	E_p^{red}		−547	−545	−546	−545	−545
III	E_p^{ox}			−869	−847	−833	−820
	E_p^{red}			−935	−933	−933	−933
IV	E_p^{ox}				−1130	−1116	−1104
	E_p^{red}				−1192	−1192	−1192
V	E_p^{ox}					−1509	−1506
	E_p^{red}					−1643	−1643
VI	E_p^{ox}						−1833
	E_p^{red}						−1936

[a] E_p^{ox} and E_p^{red} (mV) vs Fc^+/Fc; $\nu = 100$ mV s^{-1}. [b] E_p^{ox} taken as the average of the two peaks observed.

However, a new process of low current intensity appeared between processes IV and V and the oxidation component of process II was split into two components when the scan was switched at potentials more negative than process III (Figure 4a). These effects are most likely due to precipitation of mixed cation salts onto the electrode surface. The E_p^{ox} and E_p^{red} values for processes I and II (which show solution phase behavior) were slightly more negative than those found when $[bmim]^+$ was the only cation present (compare Tables 5 and 1). This is attributed to the presence of $[Bu_4N]^+$ with its weaker ion-pairing properties. It should be noted, however, that processes III−VI inclusive (which involve film formation) have E_p^{ox} and E_p^{red} values almost identical with those with $[bmim]^+$ only (compare Tables 5 and 1). Thus, the behavior could be described by Scheme 2, with the red pathway followed when the compound is reduced by three electrons and the blue pathway followed when the compound is reduced by four or more electrons.

Rotating disk electrode voltammograms were very similar to those observed when $[bmim]^+$ was the only cation present (compare Figures 4b with Figure 2a,b); i.e., two well-defined processes were observed, followed by surface-confined voltammetry upon further reduction (Figure 4). Interestingly, the potential at which the compound redissolved is more

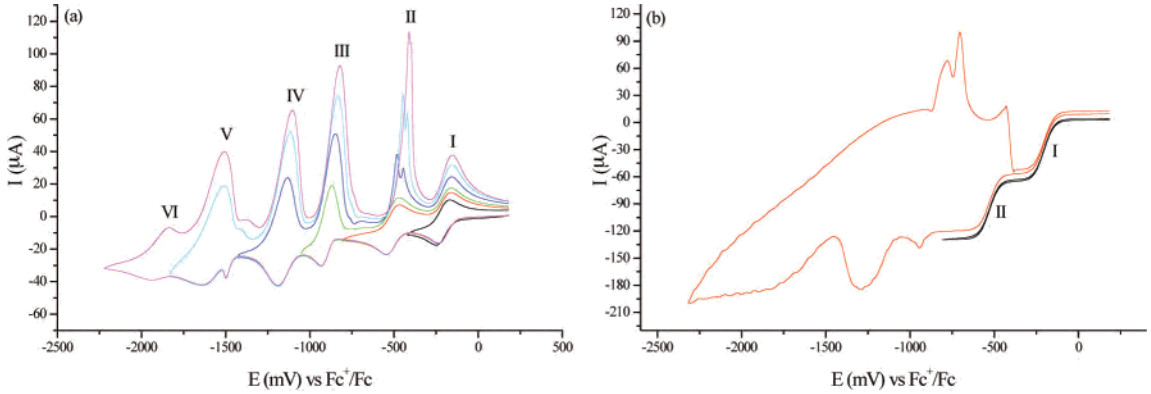

Figure 4. (a) Cyclic voltammograms (υ = 100 mV s^{-1}) when the potential was switched after the second (black), third (red), fourth (blue), and sixth (green) processes and (b) RDE voltammograms (N = 3000 rpm, υ = 10 mV s^{-1}) when the potential was switched after the second (black) and sixth (red) processes for the reduction of $[Bu_4N]_4[\alpha\text{-}S_2W_{18}O_{62}]$ (1 mM) at a glassy carbon electrode in CH_3CN ([bmim][PF_6], 0.1 M).

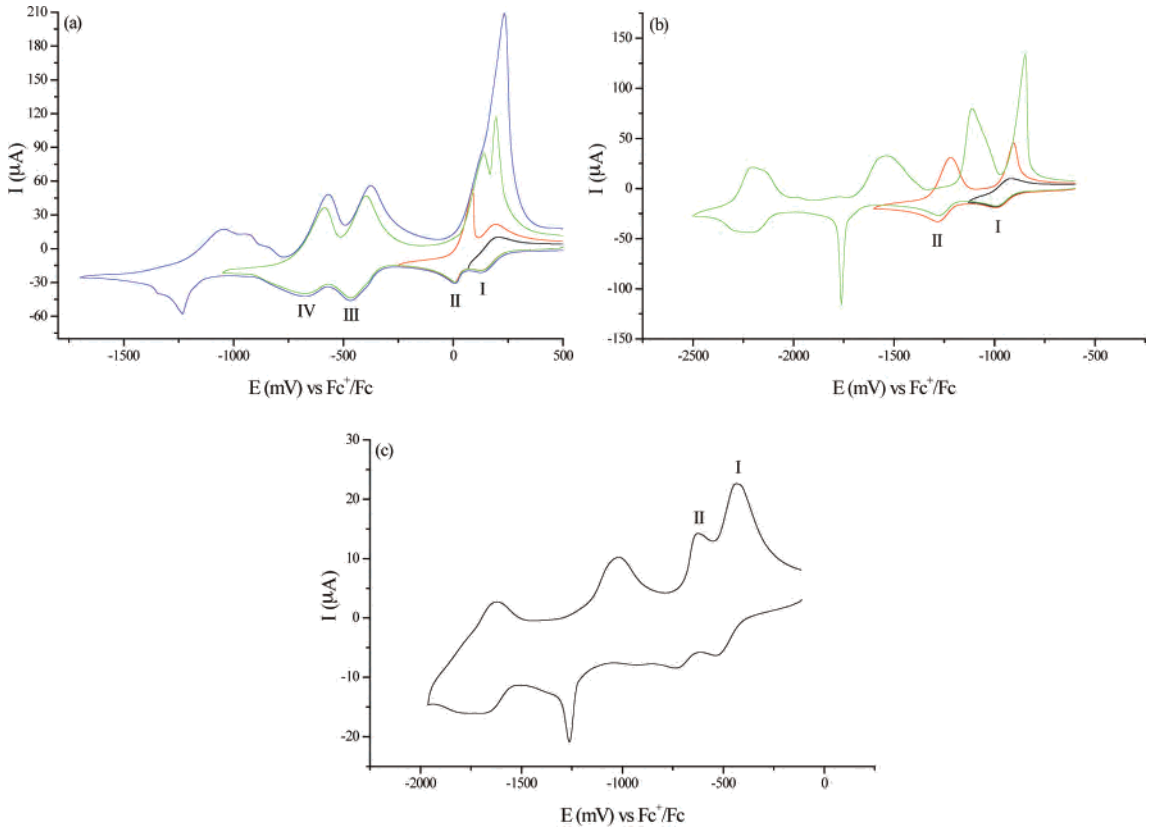

Figure 5. Cyclic voltammograms (υ = 100 mV s^{-1}) for the reduction of [bmim]$^+$ salts at a glassy carbon electron in CH_3CN ([bmim][PF_6], 0.1 M): (a) $[S_2Mo_{18}O_{62}]^{4-}$ (1 mM) when the potential was switched after the second (black), fourth (red) and sixth (blue) processes; (b) $[SiW_{12}O_{40}]^{4-}$ (1 mM) when the potential was switched after the first (black) and second processes (red) and at very negative potentials (blue); (c) [bmim]$_4$[$SiMo_{12}O_{40}$] adhered to the electrode surface.

Scheme 3

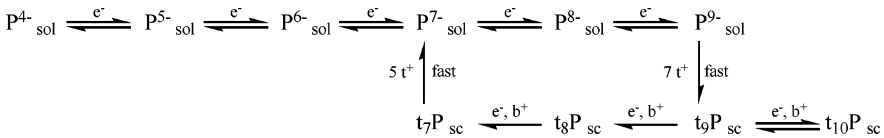

positive than when [bmim]$^+$ only is present (compare Figure 4b with Figure 2b). The impact of the presence of 0.004 M $[Bu_4N]^+$ in solution is detected in the voltammetry via increased solubility and decreased ion clustering effects.

Voltammetry of Other [bmim]$^+$ Salts in CH_3CN ([bmim][PF_6], 0.1 M). [bmim]$_4$[$S_2Mo_{18}O_{62}$]. Four well-defined processes were observed for the reduction of [bmim]$_4$[$S_2Mo_{18}O_{62}$] at a glassy carbon electrode under conditions of cyclic voltammetry (Figure 5a). E_p^{red} and E_p^{ox} values are given in Table 6. Further reduction processes were also detected at more negative potentials, but these processes are significantly more complex than the first four and are not discussed further. For the first process, the values of I_p^{ox}/I_p^{red} for all scan rates were close to unity and a plot of I_p^{red}

Table 6. Cyclic Voltammetric Data[a] for the Reduction of Solid $[bmim]^+$ Salts of $[\alpha\text{-}S_2Mo_{18}O_{62}]^{4-}$ (1 mM), $[\alpha\text{-}SiW_{12}O_{40}]^{4-}$ (1 mM), and $[\alpha\text{-}SiMo_{12}O_{40}]^{4-}$ (Solid State) in CH_3CN ($[bmim][PF_6]$, 0.1 M) at a Glassy Carbon Electrode

			process scanned to			
$[bmim]_4[POM]$	process	type	I	II	III	IV
$[\alpha\text{-}S_2Mo_{18}O_{62}]^{4-}$	I	E_p^{ox}	+207	+195	+192	+195
		E_p^{red}	+124	+124	+126	+127
	II	E_p^{ox}		+87	+65	+141
		E_p^{red}		+9	+12	+12
	III	E_p^{ox}			−418	−396
		E_p^{red}			−467	−467
	IV	E_p^{ox}				−672
		E_p^{red}				−587
$[\alpha\text{-}SiW_{12}O_{40}]^{4-}$	I	E_p^{ox}	−915	−903		
		E_p^{red}	−995	−996		
	II	E_p^{ox}		−1218		
		E_p^{red}		−1284		
$[\alpha\text{-}SiMo_{12}O_{40}]^{4-}$	I	E_p^{ox}	−442	−415		
		E_p^{red}	−544	−544		
	II	E_p^{ox}		−627		
		E_p^{red}		−735		

[a] E_p^{ox} and E_p^{red} (mV) vs Fc^+/Fc; $\upsilon = 100$ mV s^{-1}.

Table 7. Cyclic Voltammetric Data[a] for the Reduction of A^+ Salts in CH_3CN ($[A][PF_6]$, 0.1 M) at a Glassy Carbon Electrode

			process			
anion	A^+	type	I	II	III	IV
$[\alpha\text{-}SiMo_{12}O_{40}]^{4-}$	$[bmim]^+$[b]	E_p^{ox}	−415	−627		
		E_p^{red}	−544	−735		
	$[Bu_4N]^+$[c]	E_p^{ox}	−675	−1068	−1728	
		E_p^{red}	−745	−1138	−1850	
$[\alpha\text{-}SiW_{12}O_{40}]^{4-}$	$[bmim]^+$[c]	E_p^{ox}	−903	−1218		
		E_p^{red}	−996	−1284		
	$[Bu_4N]^+$[c]	E_p^{ox}	−1080	−1585	−2270	
		E_p^{red}	−1153	−1660	−2348	
$[\alpha\text{-}S_2Mo_{18}O_{62}]^{4-}$	$[bmim]^+$[c]	E_p^{ox}	+195	+141	−396	−587
		E_p^{red}	+126	+12	−467	−672
	$[Bu_4N]^+$[c]	E_p^{ox}	+143	−103	−743	−1018
		E_p^{red}	+68	−173	−833	−1113

[a] E_p^{ox} and E_p^{red} (mV) vs Fc^+/Fc; $\upsilon = 100$ mV s^{-1}. [b] Solid adhered to the electrode surface. [c] 1 mM solution.

vs $\upsilon^{1/2}$ was linear, indicating that this was a diffusion-controlled, chemically reversible process.

In contrast, when the scan range included the second reduction step, the oxidation peak associated with process II now exhibited surface confined behavior. Analogous behavior was observed for processes III and IV. However, the oxidation component of process I also appeared to exhibit surface confined characteristics when the compound was reduced by more than two electrons. Thus, the voltammetric behavior is described by Scheme 4, where the red and blue pathways are followed when the compound is reduced by two and three or more electrons, respectively. Q represents $[S_2Mo_{18}O_{62}]$, and the other terms were defined in Schemes 1−3. Reasons for this difference in behavior are not understood at present, and Scheme 4 is highly simplified.

With more extensive reduction, the potentials of the oxidation components of processes I and II became increasingly less negative, but their separation decreased. As is the case with the tungsten analogue, E_p^{red} values remained unchanged for processes I to IV, but E_p^{ox} values became

Scheme 4

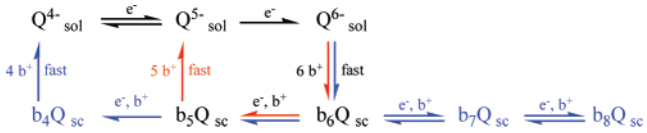

Scheme 5

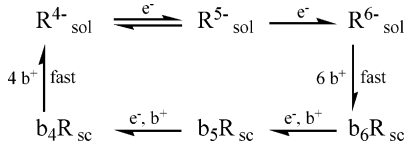

increasingly less negative for each process (Table 6). The E_p^{ox} and E_p^{red} values were also less negative than those for the $[Bu_4N]^+$ salt dissolved in CH_3CN ($[Bu_4N][PF_6]$, 0.1 M) (Table 7), an effect again attributable to the relatively weaker ion-pairing ability of the $[Bu_4N]^+$ cation. The voltammetric characteristics differed from those found for $[bmim]_4[\alpha\text{-}S_2W_{18}O_{62}]$, because $[bmim]^+$ salts of the molybdenum system were less soluble.

From the RDE data, a plot of I_L vs $\omega^{1/2}$ for the first process was linear and the diffusion coefficient was determined to be 7.3×10^{-6} cm^2 s^{-1}, similar to that of 6.4×10^{-6} cm^2 s^{-1} reported for the $[Hex_4N]^+$ salt (determined from the RDE data) dissolved in CH_3CN ($[Bu_4N][PF_6]$, 0.1 M).[40] A plot of E vs $\ln[(I_L - I)/I]$ was linear, and a value of $n = 1.0$ electron equiv was obtained from the gradient.

Reduction under RDE conditions beyond the one-electron stage again led to deposition of a condensed phase on the electrode surface. However, when the potential scan direction was reversed, the reduced surface confined solid redissolved before the onset of process I, consistent with Scheme 4. This complex voltammetry was in contrast to that found when the $[Hex_4N]^+$ salt was dissolved in CH_3CN (0.1 M $[Bu_4N][PF_6]$), where at least five well-defined solution-phase reversible, one-electron reduction events were observed.[23]

$[bmim]_4[SiW_{12}O_{40}]$. Cyclic voltammograms obtained for the reduction of $[bmim]_4[SiW_{12}O_{40}]$ (1 mM) in CH_3CN ($[bmim][PF_6]$, 0.1 M) also exhibit a well-defined initial process (Figure 5b and Table 6). A plot of I_p^{red} vs $\upsilon^{1/2}$ for process I was linear, and I_p^{ox}/I_p^{red} for all scan rates used (20−1000 mV s^{-1}) was close to unity indicating that this was a well-defined, chemically reversible process. When the scan range included the second reduction step (Figure 5b), the oxidation components of both process I and II exhibited characteristics of surface-confined voltammetry. The voltammetric behavior is described by the simplified Scheme 5, where R represents $[SiW_{12}O_{40}]$ and the other terms are defined above.

Interestingly, when surface-confined $[bmim]_6[SiW_{12}O_{40}]$-(solid) was further reduced, the voltammetry became very complex and the mechanism for reduction was probably different from that encountered in the previous examples above. A third process with a very sharp peak and broad, barely resolved fourth and fifth reduction processes were detected. Therefore, discussion is limited to processes I and II only.

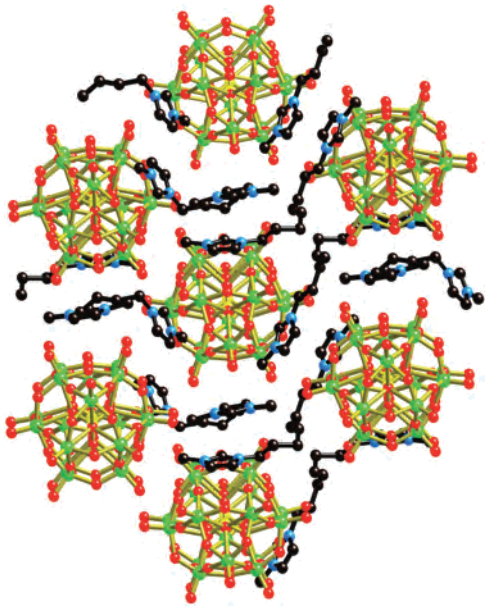

Figure 6. Packing diagram as viewed down the *b*-axis. W, S, O, N, and C atoms are in green, yellow, red, blue, and black, respectively.

Scheme 6

$$b_4A_{sc} \underset{}{\overset{e^-,\,b^+}{\rightleftharpoons}} b_5A_{sc} \overset{e^-,\,b^+}{\rightleftharpoons} b_6A_{sc}$$

As was the case with the other anions, E_p^{red} values remained essentially the same for processes I and II. However, E_p^{ox} values became less negative the further the compound was reduced (Figure 5b and Table 6). It should be noted that both the E_p^{ox} and E_p^{red} values were less negative than those found for the $[Bu_4N]^+$ salt dissolved in CH_3CN ($[Bu_4N][PF_6]$, 0.1 M) (Table 7). This difference in E_p^{ox} and E_p^{red} values is again attributed to the relatively weaker ion pairing that occurs when using $[Bu_4N]^+$ cations for both the anion and the electrolyte.

From the RDE data, a plot of I_L vs $\omega^{1/2}$ for the solution-phase process I was linear and the diffusion coefficient was determined to be 6.3×10^{-6} cm^2 s^{-1} by applying the Levich equation. This value is similar to that found for $[Bu_4N]_4$[α-$SiW_{12}O_{40}$] in CH_3CN ($[Bu_4N][PF_6]$, 0.1 M) of 5.0×10^{-6} cm^2 s^{-1}.[41] A plot of E vs $\ln[(I_L - I)/I]$ was also linear, and the number of electron equivalents transferred was determined to be 0.9 from the gradient. Reduction beyond the one-electron form under RDE conditions, as expected, led to extensive solid formation on the electrode surface, and consequently, complex RDE voltammetry was detected on the reverse scan.

$[bmim]_4[SiMo_{12}O_{40}]$ Adhered to an Electrode Surface. As this salt was too insoluble for conventional solution-phase voltammetry in CH_3CN ($[bmim][PF_6]$, 0.1 M), solid-state voltammetric techniques were applied to establish E_p^{ox} and E_p^{red} values for the reduction of $[bmim]_4[SiMo_{12}O_{40}]$ (see Experimental Section for details). Cyclic voltammograms of $[bmim]_4[SiMo_{12}O_{40}]$ adhered to a glassy carbon electrode are given in Figure 5c and data summarized in Table 6.

Analogous behavior to that for $[bmim]_4[SiW_{12}O_{40}]$ dissolved in CH_3CN ($[bmim][PF_6]$, 0.1 M) above was observed. However, processes I and II now involve exclusively surface confined species as described by Scheme 6, where A represents $[SiMo_{12}O_{40}]$ and the other terms are defined above.

E_p^{red} values remained essentially the same for processes I and II; however, E_p^{ox} values became less negative the further the compound was reduced (Figure 5c, Table 6) and both values were less negative than those found for the $[Bu_4N]^+$ salt dissolved in CH_3CN ($[Bu_4N][PF_6]$, 0.1 M) (Table 7). This difference is attributable to the weaker ion pairing ability of $[Bu_4N]^+$ relative to $[bmim]^+$.

Conclusions

The $[bmim]^+$ salts of $[SiM_{12}O_{40}]^{4-}$ and $[S_2M_{18}O_{62}]^{4-}$ (M = Mo, W) were synthesized, and a crystal structure of the $[S_2W_{18}O_{62}]^{4-}$ salt confirmed the presence of the α-isomer.

The voltammetry of $[bmim]_4[S_2W_{18}O_{62}]$ in CH_3CN ($[bmim][PF_6]$, 0.1 M) was observed to be significantly different from that of its $[Bu_4N]^+$ salt in CH_3CN ($[Bu_4N][PF_6]$, 0.1 M). Instead of six well-behaved one-electron diffusion-controlled processes, the first two reduction events only were solution processes and further reduction led to surface-confined voltammetry. Rapid precipitation and dissolution of thin films of reduced salts (or arrays of droplets or microcrystals) produced unusual voltammograms (Figure 1).

The formal reduction potential for the solution-phase process I of the $[bmim]^+$ salt was found to be more positive than that of its $[Bu_4N]^+$ analogue. These data imply that $[bmim]^+$ is more effective than $[Bu_4N]^+$ in stablizing the reduced forms via ion clustering. The packing diagram for $[bmim]_4[S_2W_{18}O_{62}]$ reveals that the imidazolium ring interacts effectively with the surface of the anion and with itself via π-stacking interactions (Figure 6).

The voltammetry of $[bmim]_4[S_2Mo_{18}O_{62}]$ and $[bmim]_4$-$[SiM_{12}O_{40}]$ (M = Mo, W) in CH_3CN ($[bmim][PF_6]$, 0.1 M) also displayed surface-confined characteristics when the compounds were reduced beyond the first reduction process. Peak potentials were again more positive than those for the respective $[Bu_4N]^+$ salts in CH_3CN ($[Bu_4N][PF_6]$, 0.1 M), consistent with the stronger ion-pairing ability of $[bmim]^+$.

An initial aim of this work was to produce ionic liquids featuring redox-active polyoxometalate anions. The oxidized forms of the present $[bmim]^+$ salts remain solid until their decomposition temperatures. However, the rapid precipitation and dissolution of the reduced forms which determine the unusual voltametric behavior seen in Figure 1, for example, are consistent with the presence of arrays of microdroplets or microcrystals on the electrode surface. The redox properties of these arrays promise application as "working salts" or "task specific ionic liquids".[36,37]

(36) Davis, J. H., Jr. *Chem. Lett.* **2004**, *33*, 1072.
(37) Lee, S. *Chem. Commun*. **2006**, 1049.

Abbreviations

Abbreviations used are as follows: $[bmim]^+$, 1-*n*-butyl-3-methylimidazolium cation; $[C_5mim]^+$, 1-*n*-pentyl-3-methylimidazolium cation; CV, cyclic voltammetry; *d*, diameter; *E*, potential; $[emim]^+$, 1-*n*-ethyl-3-methylimidazolium cation; Fc, ferrocene; *I*, current; $I_{L,}$ limiting current; *n*, number of electron equivalents, RDEV, rotating disk electrode voltammetry.

Acknowledgment. A.M.B. and A.G.W. thank the Australian Research Council for support under Grant DP0450134.

Supporting Information Available: Details of the X-ray crystal structure solution (including Tables S1 and Figures S1 and S2). This material is available free of charge via the Internet at http://pubs.acs.org.

IC062022D